Increasing soil respiration in a northern hardwood forest indicates symptoms of a changing carbon cycle

Check for updates

Angela R. Possinger [1,2,8] ✉, Charles T. Driscoll [3], Mark B. Green [4], Timothy J. Fahey [5], Chris E. Johnson [3], Mary Margaret K. Koppers [3], Lisa D. Martel [2], Jennifer L. Morse [6], Pamela H. Templer [7], Angelina M. Uribe [6], Geoffrey F. Wilson [2] & Peter M. Groffman [1,2]

Soil carbon dioxide (CO_2) flux, or soil respiration, is a critical control on net ecosystem carbon (C) balance. Using long-term (2002-2020) measurements at the Hubbard Brook Experimental Forest (New Hampshire, U.S.), we show that soil respiration rates have notably increased since ~2015. In 2020, cumulative summer respiration flux was approximately 90% higher than the average summer flux over the 2002–2015 period. The increase in soil respiration cannot be explained directly by temperature or pH change alone. We also found that heterotrophic microbial C mineralization and microbial biomass C have also increased rapidly since ~2015, pointing towards an increase in the bioavailability of organic C substrates. We suggest that these observations are consistent with a hypothetical increase in plant allocation of C belowground in response to changing climatic and soil conditions. Quantification of interactions among co-occurring global change factors (e.g., warming temperatures, increasing atmospheric CO_2, and nutrient limitation) is needed to predict how the soil C reservoir will continue to respond to global environmental changes.

U.S. forests account for a substantial proportion (80%) of North American net carbon dioxide (CO_2) sequestration[1,2]. Most (~70%) forest carbon (C) is stored belowground in root biomass, the forest floor, and mineral soils[1], so that even small percentage changes in belowground C could disproportionately impact the strength and persistence of the forest C sink. Soil respiration (the primary pathway of soil-atmosphere CO_2 exchange) is consequently a key control on long-term forest C balance. In the northeastern U.S., increasing atmospheric CO_2 concentrations, decreasing near-surface ozone concentrations, warming air temperatures, changing precipitation patterns, and decreasing acid rain interact to affect soil C and nutrient cycles in complex ways, challenging prediction of long-term forest-climate feedbacks (Fig. 1)[3–6]. Soil respiration rates may be a useful "symptom" of changes in the C cycle, as they integrate many related C cycle processes across space and time[7–9]. At the Hubbard Brook Experimental Forest (HBEF), a northern hardwood forest site in the U.S. National Science Foundation Long-Term Ecological Research (LTER) network, decades of environmental data collection and watershed-scale experimental

manipulations provide context for assessing possible changes in the trajectory of soil respiration.

At HBEF, long-term measurements of forest C and nutrient pools and fluxes provide a record of terrestrial ecosystem response to increasing atmospheric CO_2 and associated climate change. Mean annual air temperature at HBEF has increased by at least 0.1 °C decade^{-1} and annual total precipitation has increased by ~50 mm decade^{-1} (~15% total) since the 1950s (Fig. 1a, b)[10–14]. Regionally, mean annual atmospheric CO_2 concentrations increased from 379 to 423 ppm between 2002-2021 (data from Harvard Forest, Harvard, MA[15]; Fig. 1d). While leaf litter abundance, leaf area index, and live aboveground biomass at HBEF over this period have decreased or remained stable (Fig. 1e)[16–20], there has been a marked increase (30%) in evapotranspiration since the year 2000[21,22], potentially signaling a fundamental shift in plant-atmosphere exchange of water and C. Over the same period, net nitrogen (N) mineralization, N concentrations in the soil solution, and nitrous oxide (N_2O) soil-to-atmosphere fluxes have decreased, suggesting declines in N availability, a potential

[1]CUNY Advanced Science Research Center at the Graduate Center, City University of New York, New York, NY, USA. [2]Cary Institute of Ecosystem Studies, Millbrook, NY, USA. [3]Department of Civil and Environmental Engineering, Syracuse University, Syracuse, NY, USA. [4]Department of Earth, Environmental and Planetary Sciences, Case Western Reserve University, Cleveland, OH, USA. [5]Department of Natural Resources and the Environment, Cornell University, Ithaca, NY, USA. [6]Department of Environmental Science and Management, Portland State University, Portland, OR, USA. [7]Department of Biology, Boston University, Boston, MA, USA. [8]Present address: School of Plant and Environmental Sciences, Virginia Tech, Blacksburg, VA, USA. ✉e-mail: arp264@vt.edu
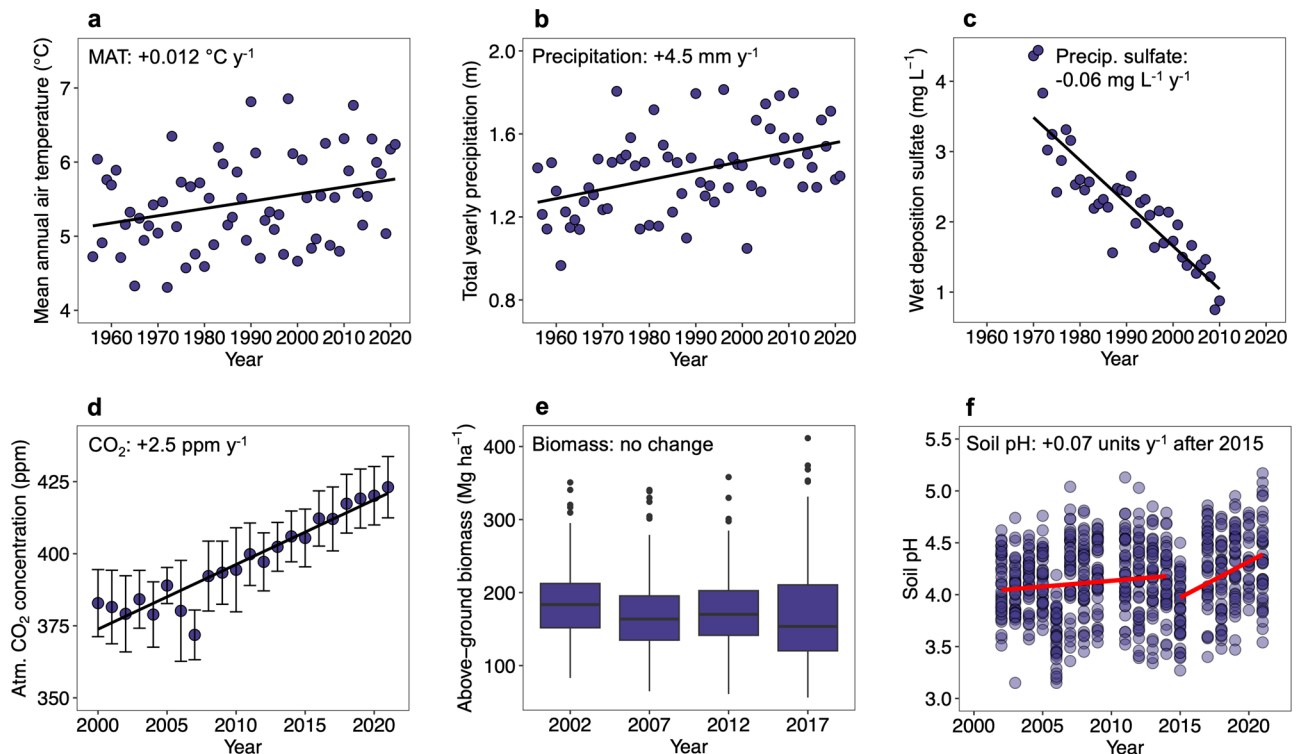
Fig. 1 | Interacting global change factors at Hubbard Brook Experimental Forest. For all plots, solid trendlines and slope estimates are included when a significant (at $\alpha = 0.05$) linear change over time was detected. **a** Air temperature at HBEF, 1956–2021 (yearly mean across all measurement stations and time intervals)[11]. **b** Annual total (cumulative) precipitation at HBEF, 1956–2021 (yearly mean across all measurement stations)[12]. **c** Wet deposition sulfate (SO_4^{2-}) concentration, 1970–2010 (yearly mean of samples collected at HBEF)[34]. **d** Northeastern U.S. regional atmospheric CO_2 concentrations (Harvard Forest, MA), 2000–2021[15]. Points and error bars represent the yearly mean ± standard deviation across all time points and two replicate sensors. **e** Aboveground live biomass at HBEF. Data are from 5-year inventories of a reference watershed (Watershed 6, 13.23 ha) and represents total living tree biomass (>10 cm diameter at breast height) for 208 inventory plots[17–20]. Boxplots show median (center line), 75th and 25th percentiles (upper and lower box edges), 1.5x the interquartile range (whiskers), and points outside 1.5x the interquartile range (points). **f** Soil pH in surface mineral soils (0–10 cm below organic horizons) collected in July of each year, including soil measurements from across both Ca-treated and reference watersheds, 4 landscape positions, and 5 replicate soil cores per landscape position ($n = 40$ pH measurements per year)[31,32].

constraint on above-ground production response to elevated CO_2[23,24]. Due to the importance of soil-atmospheric C flux in the overall C budget[25], quantifying potential changes in soil respiration flux is a critical step to constrain terrestrial feedbacks to elevated CO_2 and associated climate change drivers. Here, we use 18 years of measurements of soil CO_2 fluxes encompassing temporal variation (e.g., across seasons and years) and landscape heterogeneity (e.g., across elevation and soil property gradients) to explore where, when, and to what extent interacting global change drivers may cause important shifts in soil respiration and soil-atmosphere C feedbacks.
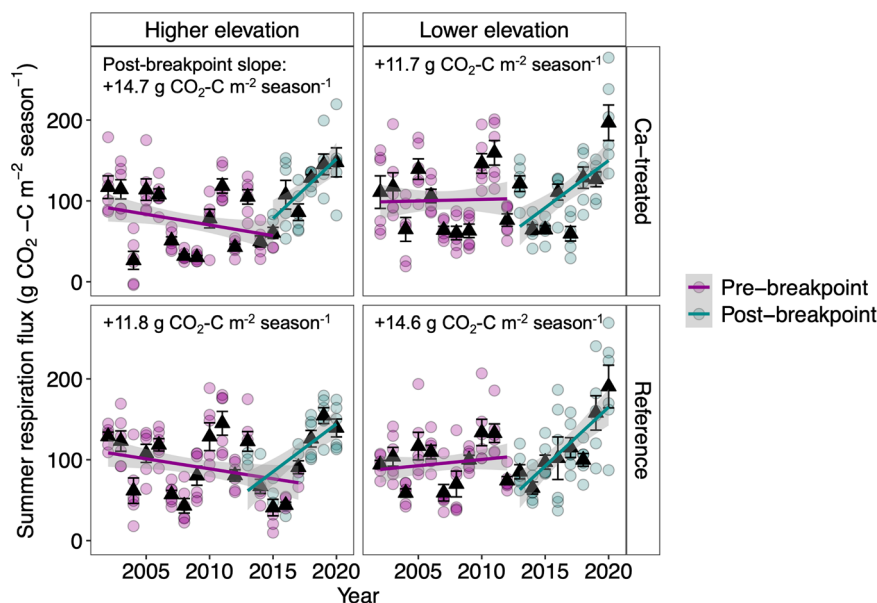
In addition to long-term ecosystem response to changing climate, experimental addition of crushed wollastonite (CaSiO$_3$, added to replace historical loss of available soil calcium (Ca) due to leaching associated with acid rain) to an experimental watershed at HBEF in 1999 provides a context for assessing soil respiration response to increased soil pH and Ca availability (Fig. 1f and Supplementary Fig. 1). Calcium addition at HBEF resulted in increases in aboveground biomass and increasing dissolved organic carbon (DOC), pH, and acid neutralizing capacity (ANC) in streamwater[26–28]. Calcium addition has also been linked to stimulation of late-stage litter decomposition[29], potentially accelerating loss of C stocks in the forest floor[30]. In addition to watershed-scale Ca treatment effects, the pH of mineral soils has increased by about 0.5 units since ~2015 as a result of overall ecosystem recovery from acid deposition in both Ca-treated and untreated watersheds, and soil solution inorganic monomeric aluminum (Al^{3+}) has decreased markedly (Fig. 1c, f, Supplementary Figs 1 and 2b)[31–34]. The ~0.5 unit increase in mineral soil pH has been associated with complex, non-linear effects on soil microbial C mineralization and N cycling[31], consistent with soil pH as an important (but

challenging to quantitatively represent) control on microbial community composition and function[35].

At HBEF, climate change and watershed experimental manipulations play out across a complex landscape template with high spatial variation in soil development[36]. In particular, upper-elevation (>~650 m elevation) soils with shallower soil profiles experience rapid water saturation cycles up to the soil surface, resulting in rapid changes in redox conditions, increasing bioavailability of soil organic matter (SOM) in mineral soils, and higher (but often more temporally dynamic) fluxes of DOC, base cations, and nitrate (NO_3^-)[36–39]. In addition to dynamic hydropedological properties, frequently saturated landscape positions often have higher, but spatially variable, densities of coniferous trees (e.g., red spruce, *Picea rubens*), which have been shown to be more responsive to environmental change than many northern hardwoods[40].

In this study, our goal was to identify whether "symptoms" of a changing C cycle could be identified at HBEF via the metric of total soil respiration. We assessed patterns in soil respiration as a function of time, Ca treatment, and elevation using long-term in-situ soil respiration measurements (2002–2020)[41] to test the hypothesis that early signs of changing soil respiration would be amplified at higher elevation landscape positions and under Ca addition. Soil respiration was measured monthly during the growing season (May–October or November) using an in-situ chamber flux method at sites distributed along elevation gradients in reference and Ca-treated watersheds at HBEF (4 landscape positions per watershed, 3 chambers per site) (Supplementary Fig. 3). We explored relationships between soil respiration and microbial biomass and microbial CO_2 mineralization using measurements of these variables[32] that were co-located with the in-situ soil respiration measurements.

Fig. 2 | Decadal-scale breakpoint in cumulative summer respiration flux. Cumulative summer (June, July, and August) soil respiration fluxes were extrapolated from monthly rate measurements[28]. Individual circular points represent three replicate collars and two landscape positions within each elevation group (n = 6 total measurements per year). Triangle points are the mean (±standard error) of all 6 measurements within a year. Individual circular point color shows the phase detected by the breakpoint algorithm for a given landscape position; point color overlaps in some cases because two landscape positions are grouped within higher and lower elevation groups. The higher elevation group includes landscape positions dominated by spruce-fir and hardwood species found at high elevation, and the lower elevation group includes sites dominated by hardwood species found at mid and low elevation (site distribution shown in Supplementary Fig. 3). Best-fit lines show a simple linear regression, and slope values are estimates of linear slope for the post-breakpoint best-fit line segment.

Results

Soil respiration is increasing across the landscape

Across both Ca-treated and reference watersheds and elevations, cumulative summer (June, July, and August) soil respiration flux increased markedly after 2013–2018 (median 2015), in sharp contrast to minimal or negative trends prior to the time series breakpoint (Fig. 2). In 2020, the overall mean summer respiration flux (~170 g CO_2-C m^{-2} $season^{-1}$) across all watersheds and elevations was approximately 90% greater than the mean summer respiration flux prior to 2015 (~ 90 g CO_2-C m^{-2} $season^{-1}$). Our observations of higher total soil CO_2 production and dissolution are consistent with increasing dissolved inorganic C (DIC) concentrations in both organic and mineral soil solutions ~2015 (Supplementary Fig. 4)[33]. Contrary to our hypothesis that the first detection of "symptoms" of the changing carbon cycle would occur at higher elevations and under Ca addition, no significant differences in slope direction and magnitude among watersheds and elevation groups were detected (linear mixed model (LMM) ANOVA, all p > 0.70) (Supplementary Table 1). The breakpoint increase in cumulative summer respiration flux was driven by increased soil respiration rates in summer, specifically in July and August (Fig. 3). We did not detect differences in post-breakpoint slope across elevation or Ca addition treatment for respiration rates (LMM ANOVA, all p > 0.60) (Supplementary Table 1).

Changes in the microbial C cycle are occurring in tandem with increasing soil respiration

Microbial biomass C, microbial biomass C:N ratio, and potential microbial C mineralization in soil samples collected in June or July also increased after ~2013–2018 (Fig. 4a–c and Supplementary Table 2). The increasing trend was strongest in Oi/Oe horizons (LMM time effect p < 0.001), followed by Oa/A horizons (LMM time effect p < 0.10), but was not statistically significant in surface mineral soils (p > 0.10) (Supplementary Table 2). These effects did not depend on Ca treatment, but varied in some cases with elevation. The increase in microbial biomass C and biomass C:N was slightly stronger, but more variable, at higher elevations, with a 30% higher slope after the breakpoint relative to lower elevations in Oi/Oe horizons (Fig. 5). In contrast, biomass specific respiration (mineralization normalized to microbial biomass) decreased after the time series breakpoint in mineral soils, suggesting an increase in microbial substrate use efficiency (Fig. 4d, Supplementary Fig. 5 and Supplementary Table 3). The change in biomass specific respiration had an inverse depth pattern: i.e., the decrease was strongest in mineral soils (p < 0.05), absent or weakly negative (after ln-transformation) in Oa/A horizons (p < 0.10), and not significant in Oi/Oe

horizons (p = 0.13) (Fig. 4d, Supplementary Table 3). Changes in biomass-specific respiration did not vary by elevation or watershed (Supplementary Fig. 5 and Supplementary Table 3).

We evaluated correlations between microbial biomass C in Oi/Oe, Oa/ A and mineral soil horizons and in-situ soil respiration rates, focusing on measurements from July (Supplementary Fig. 6). Overall, there was a strongly positive relationship between microbial biomass C and soil respiration (Spearman Rank ρ > 0.6, p < 0.001 for all horizons). However, the relationship was stronger and less variable in the pre-2015 period (ρ = 0.73–0.79) compared to 2015-present (ρ = 0.18–0.60) (Supplementary Fig. 6). In addition, in-situ soil respiration did not increase proportionally with very high microbial biomass C values (e.g., >4, 15, and 60 g MBC kg $soil^{-1}$ for mineral, Oa/A, and Oi/Oe horizons, respectively) (Supplementary Fig. 6).

Calcium addition and soil pH do not explain increase in soil respiration

In contrast to our hypothesis that Ca addition and associated deacidification would amplify soil respiration effects, we did not observe consistent differences in respiration and soil C cycling metrics as a function of Ca addition (Fig. 2, and Supplementary Tables 1–3). However, in addition to categorical differences between treated and reference watersheds, there is evidence of broader trends of increasing soil pH and decreasing soil solution inorganic monomeric aluminum (Al^{3+}) as a component of broader ecosystem recovery from acid rain at HBEF[31,33,34] and regionally[42] (Supplementary Figs 1 and 2). While soil pH dynamics over the available record (1994-2020) vary by horizon and Ca treatment, soil pH generally increased after ~2015, from an overall mean pH of 3.8 in 2015 to 4.1 in 2021 (Fig. 1f and Supplementary Fig. 1). However, there were weak or non-significant correlations between cumulative summer respiration flux and mean annual soil pH (Spearman Rank ρ = 0.31, p = 0.23) and soil solution Al^{3+} (Spearman Rank ρ = −0.41, p = 0.09) in the reference watershed across the available record (2002–2020, excluding 2016 due to lack of pH data) (Supplementary Fig. 2).

Increasing air and soil temperature, or changes in soil moisture, do not explain increasing soil respiration

Temperature is a direct and well-established control on rates of microbial C mineralization and is generally well-represented by an exponential Q_{10} response function. Bond-Lamberty et al.[43] reported global increases in soil respiration proportional to increasing air temperatures. Over the available record (1956-2021) at HBEF[11], mean annual air temperatures increased by

Fig. 3 | Decadal-scale breakpoint in soil respiration rates. Soil respiration rates were measured monthly from May to October or November (2002–2020). For all plots, points represent a soil respiration measurement at one time point for a single replicate collar, landscape position, and watershed treatment. **a** All soil respiration rates measured May-October or November. **b** Soil respiration rates from July and August only.
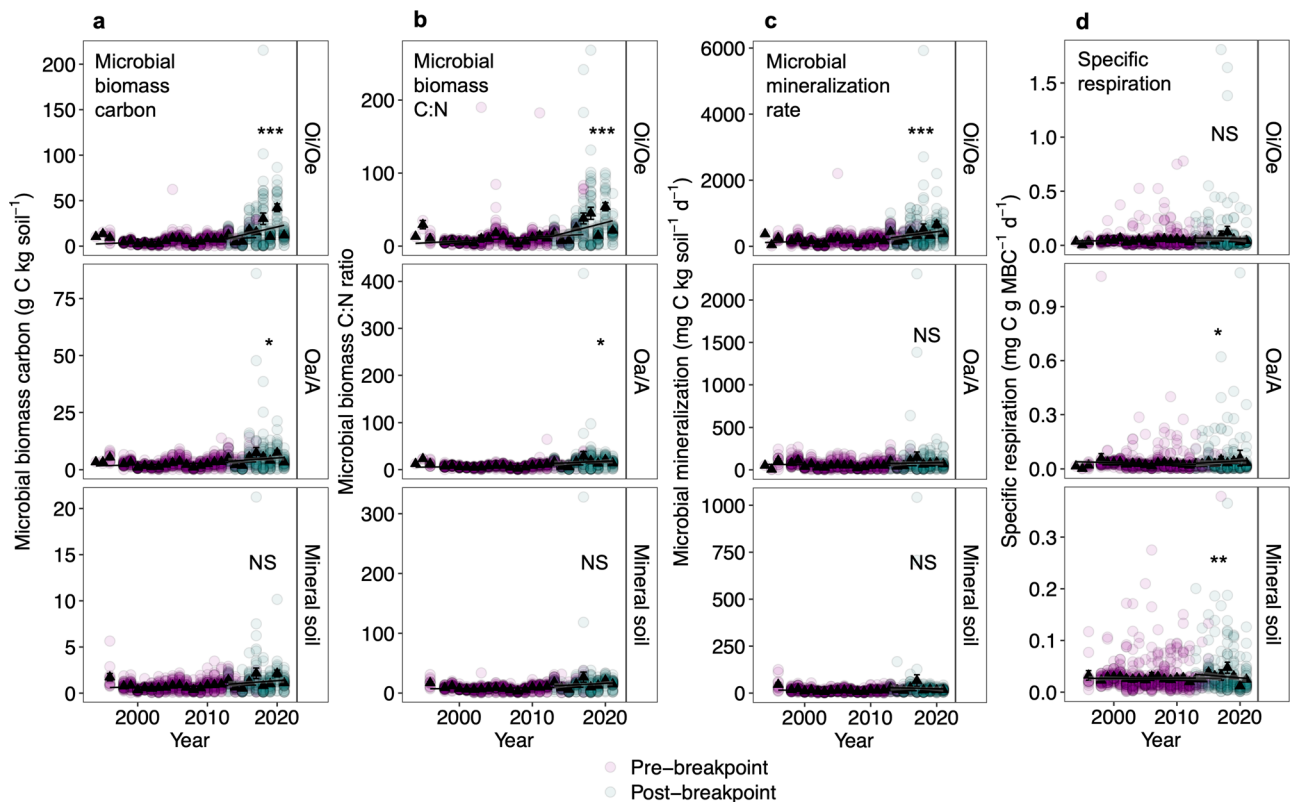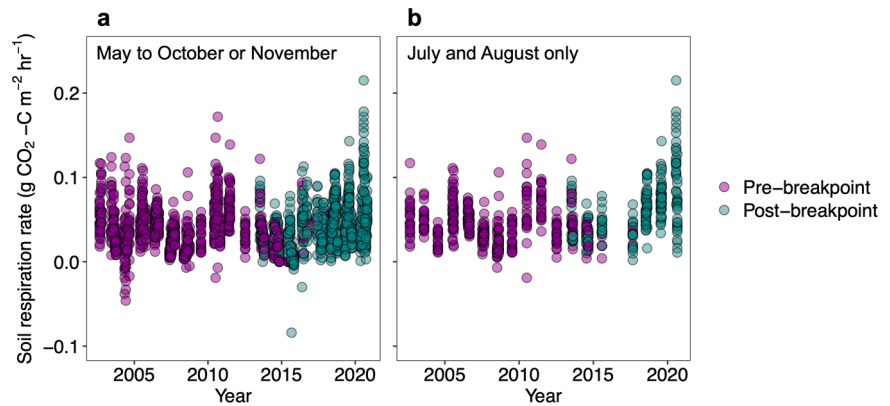

Fig. 4 | Indicators of changing microbial carbon processing in organic and mineral soils. Individual circular points represent June or July soil measurements from two watersheds, four landscape positions, and up to five replicate cores per landscape position each year ($n = 40$ points per year) within one horizon type (Oi/Oe, Oa/A, or surface mineral soil). Triangle points are the mean (± standard error) of all 40 measurements within a year. Individual circular point color shows the soil respiration period (pre- or post-breakpoint) for a given landscape position; point color overlaps in some cases because four landscape positions and watersheds are grouped within a year. Best-fit lines (for visualization only) show simple linear regression for each pre- and post-breakpoint time segment. Stars indicate linear mixed model ANOVA p-value for change in each parameter over time in the post-breakpoint phase only, where NS = $p > 0.10$, * = $p < 0.10$, ** = $p < 0.05$, and *** = $p < 0.001$ (Supplementary Tables 2 and 3). **a** Microbial biomass carbon (MBC) (chloroform-fumigation 10-d incubation); **b** Microbial biomass C:N ratio; **c** Microbial heterotrophic mineralization rate (aerobic 10-d incubation); **d** Biomass specific respiration rate (mineralized CO_2 normalized to MBC).

an average of 0.012 °C year^{-1} and summer air temperatures increased by 0.015 °C year^{-1} (Fig. 1). Using a Q_{10} range of 1.5 to 3[25,43], an increase of 0.015 °C year^{-1} in summer air temperature between 2015 and 2020 would result in a 0.3-0.8% increase in summer respiration rates, much lower than the actual increase observed (over 100%) (Fig. 3).

Soil temperature may be a more direct control on soil respiration rates and their intra-annual variation than air temperature[44,45]. To assess whether soil temperature at the time of measurement could explain increasing respiration rates, we used surface soil temperature measurements from a network of sensors distributed across the elevation gradient paired to the

date and time window (10 a.m.–4 p.m.) of soil respiration measurements (Supplementary Fig. 3)[46,47]. Because the sensors are not co-located with soil respiration collars (locations shown in Supplementary Fig. 3), we used these data as a potential reasonable range in daily minimum, maximum, and mean soil temperatures within the sampling time window, encompassing the elevation gradient used for soil respiration measurements. Since 2011 (the earliest year of soil temperature data collection in this network), minimum, maximum, and mean summer (July and August) soil temperature slightly increased, with the greatest increase in minimum soil temperature (simple linear model $p < 0.005$, slope: +0.21 °C y^{-1}) (Supplementary Fig. 7). Using

T:E interaction *p* < 0.05
Higher elev. slope = 0.13, *p* < 0.05
Lower elev. slope = 0.10, *p* < 0.05

T:E interaction *p* < 0.10
Higher elev. slope = 0.13, *p* < 0.05
Lower elev. slope = 0.10, *p* < 0.05

T:E interaction *p* = 0.28
Higher elev. slope = 0.11, *p* < 0.05
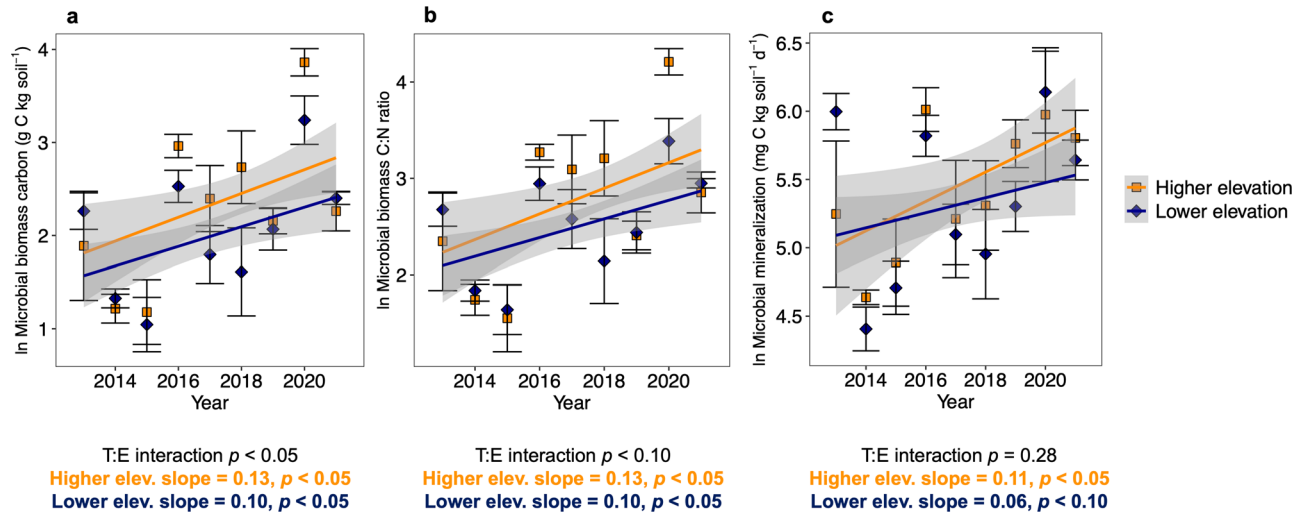**Lower elev. slope = 0.06, *p* < 0.10**

Fig. 5 | Increase in microbial carbon cycling metrics post-breakpoint in the Oi/Oe horizon. Each point is the mean of up to 5 replicate plots, 2 watersheds, and 2 landscape positions within each elevation group (higher or lower elevation; locations shown in Supplementary Fig. 3) (±standard error). Time by elevation interaction effects (T:E) are derived from linear mixed models (Supplementary Table 2). Best-fit lines and slope estimates for visualization of effect direction and magnitude are derived from simple linear regression, with shaded area indicating standard error. **a** Microbial biomass carbon (chloroform-fumigation 10-d incubation); **b** Microbial biomass C:N ratio; **c** Microbial heterotrophic mineralization rate (aerobic 10-d incubation).

+0.21 °C y^{-1} as a potential soil temperature maximum increase and a Q_{10} range of 1.5 to 3, this would equate to a 4.3–12.2% increase in respiration rate from 2015 to 2020. This increase is larger than that predicted by the increase in air temperature (0.3–0.8%), but remains small compared to the actual observed increase in respiration rate (over 100%).

Discussion
Implications of a rapid increase in soil respiration flux for forest C balance
The rapid increase in soil respiration detected in this study across all landscape positions has important implications for our understanding of the total C budget in Northeastern forests and for assessment of potential net forest C uptake. The rate and magnitude of the recent increase in soil CO_2 flux point towards disequilibrium from the antecedent steady state[25], potentially shifting the soil C flux towards a net C loss. We estimated that cumulative summer (June, July, and August) respiration increased by about 11–15 g CO_2-C m^{-2} season^{-1} since ~2015 (Fig. 2). We used this estimate to consider the magnitude of increasing soil respiration in the context of other C pools at HBEF. We estimated the forest floor C pool at HBEF to be ~2.6 kg m^{-2} using soil profile C inventories from 2014 and 2018 (conducted following methods described in Johnson et al.[30]) (Supplementary Table 4). Even as a conservative underestimate of actual flux (due to known limitations of the static chamber method)[48], the size of the summer soil respiration flux relative to the forest floor pool would increase from ~3.5% (pre-2015) to 20–30% by 2060. At the scale of the conterminous U.S., given the modest (up to 4 Tg C sequestered y^{-1})[2] estimates of net sequestration of C in the forest floor from 1990 to 2010 relative to the size of the forest floor stock (2680 Tg C)[1], an increase in soil respiration of this magnitude has the potential to reverse net sequestration in temperate forest soils.

Our results are consistent with those presented by Mann et al.[24], who reported increasing soil respiration from ~2009-present within the Multiple Element Limitation in Northern Hardwood Ecosystems (MELNHE) study at HBEF that was independent of nutrient treatment (see Fig. 7 in Mann et al.[24]). Similar to Mann et al.[24], we did not find a temperature-driven soil respiration response. In contrast to Mann et al.[24], we found a clear breakpoint increase in soil respiration, rather than a gradual increase, an observation enabled by the higher frequency of our measurements and the longer duration of our record. Our observations also showed a consistent breakpoint increase in total soil respiration across all landscape positions, encompassing known variation in vegetation and soil type.

Mann et al.[24] also found similar increases in soil respiration at other sites in the White Mountains region (Bartlett Experimental Forest, Bartlett, NH, and Jeffers Brook, Benton, NH). While datasets such as the Global Soil Respiration Database (SRDB)[49] show an increase in soil respiration CO_2 flux at a global scale[50], data coverage in the SRDB of the Northeastern US region (e.g., latitude 40 to 48° and longitude −75 to −63°) is sparse, with most observations from long-term soil respiration measurements in warming experiments at Harvard Forest (Harvard, MA). At Harvard Forest, soil respiration observations from 1992 to 2010 show no apparent trend in soil respiration over time[51], in line with HBEF observations up to 2010. To understand the extent of increasing soil respiration as a broader phenomenon, expansion of the spatial extent of long-term soil respiration measurements is needed, in combination with further synthesis of long-term data from HBEF and nearby sites with newer observations from Harvard Forest and other locations. However, observations of increasing soil respiration independent of experimental manipulation (in our study and Mann et al.[24]), as well as elevation, vegetation, or soil type in our study, point towards a possible region-wide increase in respiration flux, with profound implications for overall C cycle balance.
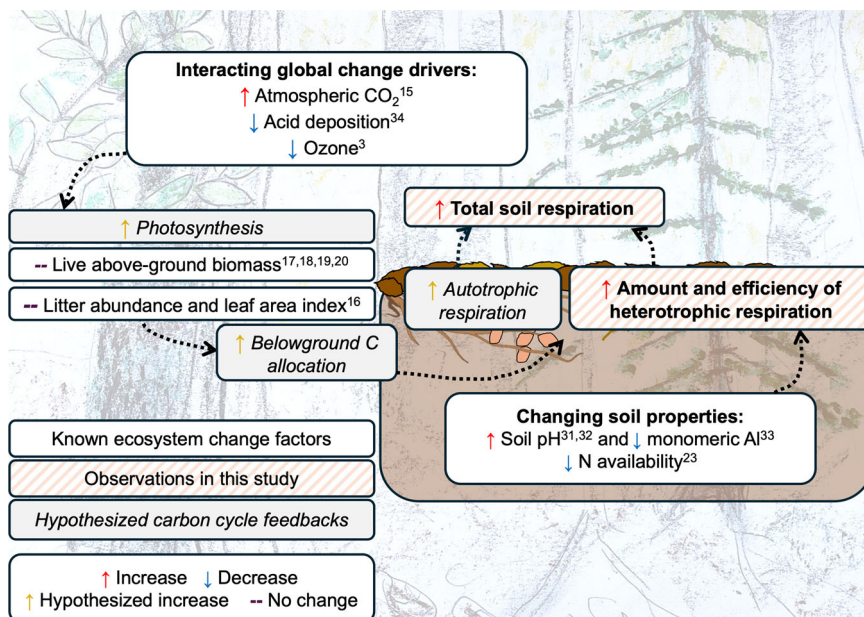
Soil pH, temperature, and moisture do not explain increases in soil respiration flux
In addition to ubiquitous increasing soil respiration since 2015 across elevations, we did not detect differences in time patterns between Ca-treated and reference watersheds. These observations are in line with prior assessment of in-situ respiration fluxes that found no change in soil respiration after Ca addition, and inconsistent or non-linear relationships between increasing soil pH and microbial C cycling processes[28,31,52], suggesting that increasing soil pH alone is not the primary driver of increasing respiration. Furthermore, we determined that the negligible increase in soil respiration explained directly by soil temperature (up to 12.2%, based on a high-end Q_{10} = 3 temperature response) excludes a simple temperature-dependent explanation for increasing soil respiration rates (over 100% increase).

In addition to soil temperature, soil moisture is a strong driver of soil respiration[53]. In generally aerobic soils, increasing soil moisture would be expected to stimulate higher soil respiration rates[53]. While we did not directly evaluate soil moisture in this study, published measurements across elevation at HBEF indicate that soil moisture decreased from 2011 to 2017[22], consistent with increases in evapotranspiration at HBEF. An increase in soil

Fig. 6 | Proposed atmospheric and soil factors contributing to increasing soil respiration flux. Co-occurrence of soil respiration changes with microbial carbon cycling parameters (increasing biomass, C:N ratio, and heterotrophic mineralization), concentration of effects in root-dense layers, and intensification of responses during the peak growing season suggest that increasing soil respiration may be driven by plant production and carbon allocation responses to interacting global change factors. Changing atmospheric factors (especially elevated CO_2) and changing soil biogeochemical cycles may increase allocation of relatively simple C substrates to the rhizosphere to stimulate, or "prime," microbial SOM turnover and mineral solubilization.

moisture can therefore not be a driver of the observed increases in soil respiration.

Plant-soil-microbial feedbacks as a proposed driver of increasing soil respiration

In lieu of clear temperature, moisture, or pH controls, we propose that the high-magnitude increase in soil respiration across the landscape is driven by interactions among below-ground C allocation, soil microbial communities, and soil organic C bioavailability (Fig. 6). One plausible mechanism is an increase in allocation of relatively simple C substrates to the rhizosphere that stimulate, or "prime," microbial SOM turnover and mineral solubilization in response to elevated CO_2 and N oligotrophication[23,54–56]. Our rationale for this mechanism is based on co-occurring changes in microbial C cycling, spatial distribution of effects across litter layers and mineral soils, and temporal concentration of effects during the peak growing season. Increased root-to-rhizosphere C flux would be consistent with the observed increase in microbial biomass C and mineralization rate primarily in Oi/Oe horizons, as well as more efficient microbial substrate mineralization in mineral horizons (e.g., from downward transport of relatively bioavailable substrates directly from exudation and/or microbially transformed SOM). Further, the increase in microbial biomass C:N is consistent with increasing fungal (possibly root-associated) contributions to microbial biomass[57,58]. In addition to soil depth patterns, the greatest increase in soil respiration rates occurred during the summer (Fig. 3), when photosynthetic rates are generally the highest in the northeastern US[59], coinciding with higher potential C allocation to fine root production[60].

In addition to evidence of these consistent spatial and temporal trends, we considered whether plant-microbial-soil feedbacks could be a plausible cause of increasing soil respiration in the context of the forest C budget, using prior estimates of root-rhizosphere C fluxes[25]. Using a mass balance approach, Fahey et al.[25] estimated a total root to rhizosphere C flux (e.g., root exudation, rhizodeposition, and allocation to mycorrhizal fungi) of $80\,g\,C\,m^{-2}\,y^{-1}$ at HBEF. In this study, the increase in soil respiration was mostly driven by summer months (Fig. 3), and we estimated cumulative summer respiration flux to be ~11–15 g CO_2-C m^{-2} season^{-1} (Fig. 2). For a change in exudate C to match this increasing respiration C flux, annual root-rhizosphere flux would need to increase by ~10–20% in summer, corresponding to an ~2–3% yearly increase in total belowground C allocation[25]. This increase could reasonably be supported by an increase in gross primary production (GPP) driven by elevated CO_2[61,62]. Increasing GPP would also be plausible based on recent

(since ~2011) rapid increases in ecosystem-scale ET[21,22] at this site. Collectively, these observations underscore the need for further studies that employ approaches coupling climate and vegetation simulations with soil C models that explicitly represent microbial C and C:N dynamics and root-rhizosphere C exchanges[63]. Incorporation of available estimates of other forest C pools and fluxes (e.g., updated forest floor stocks[30], or measurements of C turnover using radiocarbon approaches) will be necessary to constrain the potential implications of changing soil respiration fluxes. Such approaches are needed to unravel the complex interactions between changing climate, atmospheric chemistry, and ecosystem processes that are driving major changes in the Earth system.

Increasing root respiration is also consistent with increasing soil respiration rates in summer. Changing environmental controls that could influence overall production and C allocation (e.g., elevated CO_2) could also increase total autotrophic respiration[64,65] and its contribution to total soil respiration fluxes[66]. In this study, the non-linear increases in heterotrophic microbial mineralization (using laboratory assays that exclude root respiration), microbial biomass C, and microbial biomass C:N (Fig. 4) that track with patterns in soil respiration suggest that root respiration is not the primary driver of increasing soil respiration. However, the decoupling of microbial biomass with field respiration rates when microbial biomass is very high (Supplementary Fig. 6) suggests non-microbial processes may be more important under some conditions. Additionally, given the significant (>50%, with high uncertainty) contribution of root respiration to total soil respiration in this system[25], further exploration of potential changes in respiration partitioning is needed. Time series measurements of root properties and autotrophic respiration that can be meaningfully compared to long-term soil respiration measurements are not currently available at HBEF. We therefore encourage further research on drivers of increasing soil respiration tied to below-ground C allocation, including long-term fine-root biomass measurements, efforts to refine partitioning of root respiration, and development of new long-term monitoring of root-rhizosphere fluxes and root-associated microbial communities. Experiments or analysis of soil archives to track plant-derived C into soil pools using isotope approaches will also be an important direction for further evaluation of the potential for a shift in the fate of plant-derived C belowground.

Interactions among edaphic properties and ecosystem change factors may contribute to increasing soil respiration

While coupled plant production-C allocation responses may be a plausible mechanism explaining increasing soil respiration trends, potential

mechanisms contributing to higher SOM bioavailability and mineralization rates are not limited to plant-driven C allocation per se. For example, increasing C:N ratio in microbial biomass in Oi/Oe horizons—broadly consistent with increasing fungal biomass contributions[57,58]—could be related to microbial community composition changes due to interacting edaphic properties unrelated to plant C allocation. While soil pH alone was not tied directly to increasing soil respiration in this study (Supplementary Fig. 7), acid rain recovery as a broader ecosystem phenomenon influences not only soil pH, but also nutrient cation accumulation[30], Al^{3+} and DOC solubility[67–69], microbial community composition[70,71], and mycorrhizal dynamics[72], all of which could impact SOM substrate chemistry and bioavailability. While soil temperature did not directly explain the soil respiration increase during the growing season, soil warming and temperature fluctuations (particularly in winter) are likely to have cascading impacts on SOM bioavailability and microbial function[73]. Finally, while moisture content did not consistently change in a direction that could explain increasing soil respiration rates, changes in the temporal dynamics rather than the absolute soil moisture content could disproportionately influence SOM bioavailability[38]. Overall, the intensification of pH-, temperature-, and moisture-sensitive biogeochemical cycles (e.g., redox-driven changes in SOC bioavailability[36,38]) at higher elevations suggests that these landscape positions may be disproportionately influenced by ecosystem change factors that influence SOM turnover, and motivates continued monitoring of the early signs of diverging microbial C cycling processes at higher elevation identified here (Fig. 5).

Methods

Study site description

This study leverages monthly (May-October or November) soil greenhouse gas flux measurements[41] collected across an elevational gradient in two watersheds at HBEF: (1) an unmanipulated (reference) watershed (Bear Brook), from here on referred to as "reference"; (2) a watershed amended with crushed wollastonite in 1999 (Watershed 1), from here on referred to as "Ca-treated" (Supplementary Fig. 3). Both watersheds are south-facing, with average mean annual precipitation of 1400 mm, mean January temperature of −9 °C, and mean July temperature of 19 °C[10,37,74]. American beech (*Fagus grandifolia*), sugar maple (*Acer saccharum*), yellow birch (*Betula alleghe-niensis*), red spruce (*Picea rubens*), white birch (*Betula papyrifera*), and balsam fir (*Abies balsamea*) are the major tree species at HBEF. Bedrock in both watersheds is predominantly derived from Rangeley formation schist[75,76]. Wollastonite application methods in the Ca-treated watershed are described in depth in Peters et al.[77]. In brief, crushed wollastonite ($CaSiO_3$) was pelletized (~3 mm-diameter) with a lignin-sulfonate binder and applied by helicopter at a rate of ~345 g m^{-2} in 1999.

Field respiration and soil measurements were made across landscape positions categorized as low (520–560 m), mid (600–650 m), and high (725–750 m) hardwoods, and spruce-fir (770–850 m) zones (Supplementary Fig. 3). The reference watershed measurement locations coincided with long-term litter collection locations[16,78]. The Ca-treated watershed measurements were co-located with long-term soil solution chemistry (lysimeter) monitoring sites[37]. To allow for statistical contrasts, we grouped the spruce-fir and high hardwood positions as "higher" elevation and the mid- and low hardwood positions as "lower" elevation.

We used soil profile descriptions from nearby locations to categorize soil types by hydropedological unit (HPU), a detailed soil classification system developed to capture distinct soil profile characteristics driven by hydrological and transport processes in HBEF Spodosols (Supplementary Fig. 8)[36]. The higher elevation sites (high hardwood and spruce/fir landscape positions) were categorized as "Bhs podzols," which experience flashier water saturation cycles closer to the soil surface (<40 cm depth), and lateral transport of DOC, metals, and solutes from frequently saturated upslope positions[36]. The lower elevation sites (mid and low hardwood positions) were categorized as "bimodal podzols," which do not experience high frequency of saturation cycles at the soil surface and are affected by both vertical transport at the surface and lateral transport in the subsurface[36].

From here, we refer to the landscape positions by elevation group (higher or lower elevation) but emphasize that these categories are expected to coincide with divergent and spatially variable saturation and transport patterns.

In-situ trace gas analysis

Total soil respiration (CO_2 flux in g m^{-2} h^{-1}) was measured using a static chamber method[41,47,73,79]. In brief, polyvinyl chloride (PVC) rings were permanently installed to a depth of 10 cm at each sampling location ($n = 3$ chambers per site) (Supplementary Fig. 3). Measurements were collected monthly from May through October prior to 2014, and May through October or November after 2014. For measurement, a 28.7 cm-diameter by 4 cm-height polyvinyl chloride (PVC) chamber was affixed to the permanent rings. The integrity of permanent rings was periodically assessed by installing additional temporary new collars (see Supplementary Methods). Gas samples (9 mL) were collected at $t = 0$, 10, 20, and 30 min via gas sampling ports and stored in evacuated gas vials at room temperature prior to analysis. Gas samples were analyzed by gas chromatography (GC) with thermal conductivity detection, using a Shimadzu GC-14 (2002–2015) or Shimadzu GC-2014 (2015–2020) instrument (Shimadzu Corp., Kyoto, Japan). Sampling trip standards and certified external calibration standards were used to verify that instrument bias did not affect gas measurements over time (see Supplementary Methods).

Flux data were screened for outlier timepoints (6 times higher or lower than other timepoint measurements) or clear contradiction of the time trend. Fluxes were then determined based on the linear relationship between CO_2 concentration and measurement time, accounting for chamber internal volume and soil surface area.

To provide an estimate of cumulative summer respiration flux, the monthly rate measurements (g CO_2 m^{-2} h^{-1}) were extrapolated to 30 d increments (g CO_2 m^{-2} 30 d^{-1})[28] for June, July, and August. We used these months because they accounted for the most continuous record over the measurement period, and the strongest increase in respiration rates was found in summer (see Fig. 3). To account for missing combinations of elevations and sites in certain years, missing monthly measurements were gap-filled using the mean summer monthly flux. These values were summed to produce cumulative summer soil respiration fluxes. The static chamber method results in known underestimation of true soil respiration fluxes due to inherent feedbacks within the closed chamber[48]. Further, the 30-d extrapolation with gap-filling is a coarse estimate of cumulative fluxes, though represents internally-consistent changes over time[28]. However, we emphasize that these methodological considerations are more conservative with respect to the detection of trends in soil respiration and implications of changing fluxes for overall forest C balance.

Soil and soil organic matter analysis

We compared soil respiration data with data on soil microbial biomass and activity collected from 2002 to 2020 at the same locations[32]. Soil cores were collected within 20 m of each gas sampling collar annually in June or July using a 5 cm-diameter split PVC corer. Cores were collected to 10–15 cm depth, and separated into three depths, defined in the field as Oi/Oe, Oa/A, and mineral soil horizons based on degree of organic matter decomposition and mineral soil content. At each landscape position, material was composited by horizon for five replicate measurement plots (2–8 cores composited per plot).

Detailed methods for soil analysis are described in ref. 32. Briefly, soils were stored at 4 °C and field moisture content for less than three weeks prior to laboratory analyses. Soils were manually homogenized: all large rocks, roots, and other non-decomposed organic material were removed, and samples were thoroughly mixed. Gravimetric moisture content was determined by weight difference after oven-drying at 60 °C for 48 h, and all results are expressed on an oven-dry weight basis. Soil pH was determined in deionized water at a 1:2 (Oa/A and mineral soil horizons) or 1:4 (Oi/Oe horizons) soil:water ratio. Microbial biomass C and N content were measured using the chloroform fumigation-10-d incubation method[80,81], and microbially mineralized CO_2 was measured in a 10-d incubation at room

temperature (a non-fumigated incubation control). The headspace of the incubation vessels was sampled by syringe. Headspace air samples were stored in evacuated vials and then analyzed by gas chromatography with thermal conductivity detection, using a Shimadzu GC-14 (2002–2015) or Shimadzu GC-2014 (2015–2020) instrument (Shimadzu Corp., Kyoto, Japan). Biomass specific respiration was calculated by normalizing mineralized CO_2 normalized to microbial biomass C.

Environmental variables

Air temperature. Daily air temperature data were derived from the long-term (1955–2022) record, with measurements collected at up to 7 locations across the HBEF[11]. For this study, we used years with complete data (1956–2021) to calculate the yearly average across all locations, either across the entire year (i.e., mean annual temperature) or for the months of July and August only.

Precipitation. Daily precipitation data were derived from the long-term (1956–2022) complete record at HBEF, with up to 24 stations prior to 2015 and up to 10 stations after 2015[12]. The yearly average across all stations was summed within each year with complete data (1956–2021) to calculate yearly total precipitation.

Atmospheric carbon dioxide concentrations. We used atmospheric CO_2 measurements collected at the Harvard Forest EMS Tower (HFR1, US-Ha1) affiliated with the AmeriFlux network[15]. We calculated the yearly mean of two measured values at the site[82].

Wet deposition sulfate concentration. To illustrate decreasing acid rain trends over time, we used long-term monthly wet deposition chemistry measurements collected at HBEF[34]. We calculated the yearly mean across all measurement timepoints.

Soil temperature. We used in situ soil temperature measurements collected as part of an elevation and climate gradient study[46,47]. We used 6 south-facing sensor locations overlapping with the elevation range of our studied transects (Supplementary Fig. 3). At each location, two replicate soil temperature sensors were installed to a depth of 5 cm (Decagon Model 5TM, METER Group, Pullman, WA, USA) and measurements recorded hourly. For this study, we calculated average (across $n = 2$ sensors) hourly soil temperature across the available record (2011–2021). We paired soil respiration and soil temperature measurement dates, and filtered soil temperatures to the time of soil respiration collar sampling (10 a.m.–4 p.m.). We determined minimum, maximum, and mean soil temperature across hourly measurements within each measurement day and across all six measurement locations (Supplementary Fig. 3) to capture the full range of soil temperature conditions within a given sampling day. It should be noted that the available soil temperature measurements are not co-located with soil respiration collars, so they represent a potential maximum range of soil temperatures across landscape positions on a soil respiration measurement day. Therefore, we focused our analysis on the potential reasonable magnitude of soil temperature effects on soil respiration based on known biological relationships (i.e., Q_{10} temperature response functions) (see **Data analysis** section below) rather than direct correlations between soil temperature and soil respiration measurements.

Soil solution dissolved inorganic carbon (DIC) and monomeric Al. We used measurements of freely-draining soil solution DIC[33] to verify an increase consistent with increasing soil CO_2 production and dissolution in soil pore water. In addition, we used total monomeric Al concentration in soil solutions to illustrate overall ecosystem acid rain recovery trends[33]. Lysimeter installation and sampling methods are described in refs. 33,37. Soil solution DIC was determined using infrared detection, and total monomeric Al was determined using pyrocatechol violet colorimetric analysis[83].

Aboveground biomass. We used long-term estimates of above-ground biomass (living trees DBH $\geq$ 10 cm) (Fig. 1e) for a reference watershed at HBEF (Watershed 6)[17–20]. In each measurement year (2002, 2007, 2012, and 2017), DBH was measured on all trees DBH $\geq$ 10 cm in 208 plots (625 m^2). Standing and downed dead trees were excluded from the dataset. Estimates of individual tree biomass were derived from HBEF-specific allometric equations[17–20].

Forest floor C stocks. To provide context for the change in respiration relative to other C pools at HBEF, we estimated the forest floor C pool at HBEF using soil profile C inventories from 2014 to 2018 in the Ca-treated watershed (Supplementary Table 4). The Ca-treated watershed was used due the availability of data for both 2014 and 2018 (the most recent complete sampling years). Soils were excavated at 100 sites in each sampling year using a pin-block method[30]. At each site, samples of the combined Oi and Oe ("Oie") and of the Oa horizon were collected. The C pool at each site was calculated using the soil mass per unit area and the C content, measured by combustion-gas chromatography. Further details may be found in ref. 30.

Data analysis

All statistical analyses were conducted using R v. 4.0.2 in RStudio v. 1.1.423[84,85]. The base R *stats* package[84] was used unless otherwise noted.

Structural change: breakpoint detection. We identified breakpoints in soil respiration rate time series data over the 2002–2020 measurement period using the "breakpoints" function in the *strucchange* package[86,87] set a priori to detect one breakpoint in the time series, with a minimum of 20 observations in each identified time section. To determine whether the breakpoint model improved fit relative to a non-breakpoint model, we compared residual sum of squares (RSS) values with and without a breakpoint (Supplementary Fig. 9). To include sufficient observations for operability of the breakpoint algorithm, we used all replicate gas collar observations ($n = 3$ per landscape position by watershed combination). We used the identified breakpoint date from pooled soil respiration rate data to separate other time series into pre- and post-breakpoint segments, including: (1) cumulative summer CO_2 flux; (2) microbial biomass C and C:N ratio; (3) potential microbial mineralization rate; and (4) biomass specific respiration.

Ca treatment and elevation contrasts. We compared the magnitude of change over time as a function of Ca treatment and elevation in several ways. We tested for differences across Ca treatment and elevation in the post-breakpoint slope using a linear mixed model approach ("lme" function in the *nlme* package)[88]. We accounted for autocorrelation in the time series by using a continuous autoregressive (1st order) correlation structure[88]. The model included sampling year as a fixed effect, sampling year-by-elevation group (higher or lower) and sampling year-by-Ca treatment as interaction effects, and elevation (low, high, mid, and spruce-fir) as a random effect (i.e., as a measurement unit in a repeated measures sampling design). Microbial biomass C, microbial biomass C:N, microbial mineralization, and biomass-specific respiration were *ln*-transformed to increase the normality of model residuals. We also qualitatively compared the increase in soil respiration in post-breakpoint time segments by estimating slope with a simple linear model (Fig. 2).

Correlations with soil pH and microbial biomass C. The direction and magnitude of relationships between soil respiration flux and soil pH and microbial biomass C across the available measurement record were determined using Spearman rank correlation without continuity correction. For microbial biomass C, we also determined the direction and magnitude of the correlation for soil horizons (Oi/Oe, Oa/A, and mineral soils) and the pre-2015 and 2015 periods separately.

Air and soil temperature predictions. To test if increasing respiration post-breakpoint could be explained by increasing air and soil temperature temperatures alone, we determined the overall change in July and August mean air or soil temperature over the available record using a simple linear regression, and used the slope (air temperature: $+0.015\,°C\,year^{-1}$, soil temperature: up to $+0.21\,°C\,year^{-1}$, based on minimum daily temperature within the sampling time window) to predict the potential change in respiration rate with a simple Q_{10} function, starting with the overall average respiration rate in 2015 ($0.0430\,g\,CO_2$-$C\,m^{-2}\,h^{-1}$) (Fig. 3) as the initial rate. Using $Q_{10} = 1.5$ or 3.0, the predicted increase based on air temperature was to 0.0432 or $0.0434\,g\,CO_2$-$C\,m^{-2}\,h^{-1}$ (a 0.3 or 0.8% increase). Based on soil temperature, the predicted increase was to 0.0441 or $0.0459\,CO_2$-$C\,m^{-2}\,h^{-1}$ (a 4.3 or 12.2% increase). The actual mean respiration rate in 2020 was $0.092\,g\,CO_2$-$C\,m^{-2}\,h^{-1}$, an over 100% increase.

Reporting summary

Further information on research design is available in the Nature Portfolio Reporting Summary linked to this article.

Data availability

The soil and site characterization datasets used for all analyses in this study are available through the open access Hubbard Brook Data Catalog, hosted by the Environmental Data Initiative (https://hubbardbrook.org/data-catalog/).

Code availability

Data processing and statistical analysis code are publicly available at https://github.com/arp264/HBEF_soil_respiration.

References

1. Domke, G. et al. Chapter 9: Forests. In *Second State of the Carbon Cycle Report (SOCCR2): A Sustained Assessment Report* (eds. Cavallaro, N. G. et al.), 365–398 (Washington, DC: U.S. Global Change Research Program, 2018).
2. Woodbury, P. B., Smith, J. E. & Heath, L. S. Carbon sequestration in the U.S. forest sector from 1990 to 2010. *Forest Ecol. Manag.* **241**, 14–27 (2007).
3. Parrish, D. D. & Ennis, C. A. Estimating background contributions and US anthropogenic enhancements to maximum ozone concentrations in the northern US. *Atm. Chem. Phys.* **19**, 12587–12605 (2019).
4. Hayhoe, K. et al. Past and future changes in climate and hydrological indicators in the US Northeast. *Clim. Dyn.* **28**, 381–407 (2007).
5. Gilliam, F. S. et al. Decreased atmospheric nitrogen deposition in eastern North America: predicted responses of forest ecosystems. *Environ. Pollut.* **244**, 560–574 (2019).
6. Harms, T. K. et al. Patterns and trend of organic matter processing and transport: insights from the US long-term ecological research network. *Clim. Chang. Ecol.* **2**, 100025 (2021).
7. Davidson, E. A., Janssens, I. A. & Luo, Y. On the variability of respiration in terrestrial ecosystems: moving beyond Q_{10}. *Glob. Chang. Biol.* **12**, 154–164 (2006).
8. Trumbore, S. Carbon respired by terrestrial ecosystems – recent progress and challenges. *Glob. Chang. Biol.* **12**, 141–153 (2006).
9. Rodeghiero, M. & Cescatti, A. Spatial variability and optimal sampling strategy of soil respiration. *For. Ecol. Manag.* **225**, 106–112 (2008).
10. Campbell, J. L. et al. Long-term trends from ecosystem research at the Hubbard Brook Experimental Forest (No. NRS-GTR-17). U.S. Department of Agriculture, Forest Service (2007).
11. USDA Forest Service, Northern Research Station. Hubbard Brook Experimental Forest: Daily Temperature Record, 1955 - present ver 11. Environmental Data Initiative https://doi.org/10.6073/pasta/e51ee820bb04aace06fa35c00946b050 (2022).
12. USDA Forest Service, Northern Research Station. Hubbard Brook Experimental Forest: Daily Precipitation Rain Gage Measurements, 1956 - present ver 18. Environmental Data Initiative https://doi.org/10.6073/pasta/aed7e68772106753f3c7deef4f75e09c (2022).
13. Campbell, J. L. et al. Past and projected future changes in snowpack and soil frost at the Hubbard Brook Experimental Forest, New Hampshire, USA. *Hydrol. Process.* **24**, 2465–2480 (2010).
14. Hamburg, S. P., Vadeboncoeur, M. A., Richardson, A. D. & Bailey, A. S. Climate change at the ecosystem scale: a 50-year record in New Hampshire. *Clim. Change* **116**, 457–477 (2013).
15. Munger, J. W. AmeriFlux BASE US-Ha1 Harvard Forest EMS Tower (HFR1), Ver. 19-5, AmeriFlux AMP https://doi.org/10.17190/AMF/1246059 (2022).
16. Fahey, T. J., Cleavitt, N. L. & Battles, J. J. Long term variation of leaf abundance in a northern hardwood forest. *Ecol. Indic.* **137**, 108746 (2022).
17. Battles, J. et al. Forest Inventory of a Northern Hardwood Forest: Watershed 6, 2002, Hubbard Brook Experimental Forest, ver 8. Environmental Data Initiative https://doi.org/10.6073/pasta/bb0e2c20752780c97b63b5544c1aba60 (2019).
18. Battles, J. et al. Forest Inventory of a Northern Hardwood Forest: Watershed 6 2007, Hubbard Brook Experimental Forest, ver 2. Environmental Data Initiative https://doi.org/10.6073/pasta/6a1cd73c4e196f930eda7d8e25bb69d8 (2019).
19. Battles, J. et al. Forest Inventory of a Northern Hardwood Forest: Watershed 6, 2012, Hubbard Brook Experimental Forest, ver 2. Environmental Data Initiative https://doi.org/10.6073/pasta/b356ff76e03f661c581262658834a7c7 (2019).
20. Battles, J. et al. Forest Inventory of a Northern Hardwood Forest: Watershed 6, 2017, Hubbard Brook Experimental Forest, ver 1. Environmental Data Initiative https://doi.org/10.6073/pasta/0593ba15fb76a4f085797126a1bea3a7 (2019).
21. Vadeboncoeur, M. A. et al. Systematic variation in evapotranspiration trends and drivers across the Northeastern United States. *Hydrol. Process.* **32**, 3547–3560 (2018).
22. Green, M. B. et al. A catchment water balance assessment of an abrupt shift in evapotranspiration at the Hubbard Brook Experimental Forest, New Hampshire, USA. *Hydrol. Process.* **36**, e14300 (2021).
23. Groffman, P. M. et al. Nitrogen oligotrophication in northern hardwood forests. *Biogeochemistry* **141**, 523–539 (2018).
24. Mann, T. A., Yanai, R. D., Fahey, T. J. & Reinmann, A. B. Nitrogen and phosphorus addition affect soil respiration in northern hardwood forests. *Ecosyst.* **27**, 765–778 (2024).
25. Fahey, T. J. et al. The biogeochemistry of carbon at Hubbard Brook. *Biogeochemistry* **75**, 109–176 (2005).
26. Cho, Y., Driscoll, C. T., Johnson, C. E., Blum, J. D. & Fahey, T. J. Watershed-level responses to calcium silicate treatment in a northern hardwood forest. *Ecosyst.* **15**, 416–434 (2012).
27. Battles, J. J., Fahey, T. J., Driscoll, C. T., Blum, J. D. & Johnson, C. E. Restoring soil calcium reverses forest decline. *Environ. Sci. Technol. Lett.* **1**, 15–19 (2014).
28. Taylor, L. L. et al. Increased carbon capture by a silicate-treated forested watershed affected by acid deposition. *Biogeosciences* **18**, 169–188 (2021).
29. Lovett, G. M., Arthur, M. A. & Crowley, K. F. Effects of calcium on the rate and extent of litter decomposition in a northern hardwood forest. *Ecosyst.* **19**, 87–97 (2016).
30. Johnson, C. E., Driscoll, C. T., Blum, J. D., Fahey, T. J. & Battles, J. J. Soil chemical dynamics after calcium silicate addition to a northern hardwood forest. *Soil Sci. Soc. Am. J.* **78**, 1458–1468 (2014).
31. Ontman, R., Groffman, P. M., Driscoll, C. T. & Cheng, Z. Surprising relationships between soil pH and microbial biomass and activity in a northern hardwood forest. *Biogeochemistry* **163**, 265–277 (2023).
32. Groffman, P. M. & Martel, L. D. Long-term measurements of microbial biomass and activity at the Hubbard Brook Experimental Forest, 1994

Article

– present ver 23. Environmental Data Initiative https://doi.org/10.6073/pasta/aff4a2074fd56102f62f13a19ce46f2d (2021).

33. Driscoll, C. T. Chemistry of freely-draining soil solutions at the Hubbard Brook Experimental Forest, Watershed 6, 1982 - present ver 18. Environmental Data Initiative https://doi.org/10.6073/pasta/bd7ba65a4b703760c82c4e16fe494fb6 (2022).

34. Likens, G. Chemistry of Bulk Precipitation at Hubbard Brook Experimental Forest, 1969 - present, Robert S. Pierce Ecosystem Laboratory Facility ver 8. Environmental Data Initiative https://doi.org/10.6073/pasta/49b5c122f2c94353e3271152c6e869c6 (2019).

35. Fierer, N., Strickland, M. S., Liptzin, D., Bradford, M. A. & Cleveland, C. C. Global patterns in belowground communities. *Ecol. Lett.* **12**, 1238–1249 (2009).

36. Bailey, S. W., Brousseau, P. A., McGuire, K. J. & Ross, D. S. Influence of landscape position and transient water table on soil development and carbon distribution in a steep, headwater catchment. *Geoderma* **226-227**, 279–289 (2014).

37. LoRusso, N. A., Bailey, S. W., Zeng, T., Montesdeoca, M. & Driscoll, C. T. Dissolved organic matter dynamics in reference and calcium silicate-treated watersheds at Hubbard Brook Experimental Forest, NH, USA. *J. Geophys. Res. Biogeosci.* **126**, e2021JG006352 (2021).

38. Possinger, A. R. et al. Organo-mineral interactions and soil carbon mineralizability with variable saturation cycle frequency. *Geoderma* **375**, 114483 (2020).

39. Pardo, L. H., Green, M. B., Bailey, S. W., McGuire, K. J. & McDowell, W. H. Identifying controls on nitrate sources and flowpaths in a forested catchment using a hydropedological framework. *J. Geophys. Res. Biogeosci.* **127**, e2020JG006140 (2022).

40. Wason, J. W., Beier, C. M., Battles, J. J. & Dovciak, M. Acidic deposition and climate warming as drivers of tree growth in high-elevation spruce-fir forests of the northeastern US. *Front. For. Glob. Chang.* **2**, 63 (2019).

41. Groffman, P. M. & Martel, L. D. Hubbard Brook Experimental Forest: soil-atmosphere fluxes of carbon dioxide, nitrous oxide and methane on Watershed 1 and Bear Brook ver 12. Environmental Data Initiative https://doi.org/10.6073/pasta/140e9b608fe77efd595d1a243811d02b (2021).

42. Oulehle, F. et al. Major changes in forest carbon and nitrogen cycling caused by declining sulphur deposition. *Glob. Change Biol.* **17**, 3115–3129 (2011).

43. Bond-Lamberty, B. & Thomson, A. Temperature-associated increases in the global soil respiration record. *Nature* **464**, 579–582 (2010).

44. Lloyd, J. & Taylor, J. A. On the temperature dependence of soil respiration. *Func. Ecol.* **8**, 315–323 (1994).

45. Frey, S. D., Drijber, R., Smith, H. & Melillo, J. J. S. B. Microbial biomass, functional capacity, and community structure after 12 years of soil warming. *Soil Biol. Biochem.* **40**, 2904–2907 (2008).

46. Groffman, P. M., Duran, J., Morse, J. L., Wilson, G. F. & Green, M. B. Soil temperature along an elevation gradient at the Hubbard Brook Experimental Forest, 2010 - present ver 1. Environmental Data Initiative https://doi.org/10.6073/pasta/85dbc546191e92dad23077acc90a4bf (2022).

47. Wilson, G. F. et al. Snowpack affects soil microclimate throughout the year. *Clim. Chang.* **163**, 705–722 (2020).

48. Davidson, E. A., Savage, K., Verchot, L. V. & Navarro, R. Minimizing artifacts and biases in chamber-based measurements of soil respiration. *Agric. For. Meteor.* **113**, 21–37 (2002).

49. Jian, J. et al. A restructured and updated global soil respiration database (SRDB-V5). *Earth Syst. Sci. Data* **13**, 255–267 (2021).

50. Bond-Lamberty, B., Bailey, V. L., Chen, M., Gough, C. M. & Vargas, R. Globally rising heterotrophic respiration over recent decades. *Nature* **560**, 80–83 (2018).

51. Giasson, M.-A. et al. Soil respiration in a northeastern US temperate forest: a 22-year synthesis. *Ecosphere* **4**, 1–28 (2013).

52. Groffman, P. M., Hardy, J. P., Fisk, M. C., Fahey, T. J. & Driscoll, C. T. Climate variation and soil carbon and nitrogen cycling processes in a northern hardwood forest. *Ecosyst.* **12**, 927–943 (2009).

53. Hawkes, C. V., Waring, B. G., Rocca, J. D. & Kivlin, S. N. Historical climate controls soil respiration responses to current soil moisture. *Proc. Nat. Acad. Sci. USA* **114**, 6322–6327 (2017).

54. Dong, J. et al. Impacts of elevated CO_2 on plant resistance to nutrient deficiency and toxic ions via root exudates: a review. *Sci. Tot. Environ.* **754**, 142434 (2021).

55. Mason, R. E. et al. Evidence, causes, and consequences of declining nitrogen availability in terrestrial ecosystems. *Science* **376**, eabh3767 (2022).

56. Gojon, A. et al. The decline of plant mineral nutrition under rising CO_2: physiological and molecular aspects of a bad deal. *Trends Plant Sci.* **28**, 185–198 (2022).

57. Joergensen, R. G., Mäder, P. & Fließbach, A. Long-term effects of organic farming on fungal and bacterial residues in relation to microbial energy metabolism. *Biol. Fertil. Soils* **46**, 303–307 (2010).

58. Strickland, M. S. & Rousk, J. Considering fungal:bacterial dominance in soils – Methods, controls, and ecosystem implications. *Soil Biol. Biochem.* **42**, 1385–1395 (2010).

59. Wu, C., Munger, J. M., Niu, Z. & Kuang, D. Comparison of multiple models for estimating gross primary production using MODIS and eddy covariance data in Harvard Forest. *Remote Sens. Environ.* **114**, 2925–2939 (2010).

60. Pritchard, S. G. et al. Fine root dynamics in a loblolly pine forest are influenced by free-air CO_2 enrichment: a six-year minirhizotron study. *Glob. Chang. Biol.* **14**, 588–602 (2008).

61. Taiz, L. & Zeiger, E. *Plant Physiology* (The Benjamin/Cummings Pub. Co., Redwood City, California, 1991).

62. Rogers, H. H., Runion, G. B. & Krupa, S. V. Plant responses to atmospheric CO_2 enrichment with emphasis on roots and the rhizosphere. *Environ. Pollut.* **83**, 155–189 (1994).

63. Sulman, B. N., Phillips, R. P., Oishi, A. C., Shevliakova, E. & Pacala, S. W. Microbe-driven turnover offsets mineral-mediated storage of soil carbon under elevated CO_2. *Nature Clim. Chang.* **4**, 1099–1102 (2014).

64. Nie, M., Lu, M., Bell, J., Raut, S. & Pendall, E. Altered root traits due to elevated CO2: a meta-analysis. *Glob. Ecol. Biogeo.* **22**, 1095–1105 (2013).

65. Janssens, I. A., Crookshanks, M., Taylor, G. & Ceulemans, R. Elevated atmospheric CO2 increases fine root production, respiration, rhizosphere respiration, and soil CO2 efflux in Scots pine seedlings. *Glob. Chang. Biol.* **4**, 871–878 (1998).

66. Schmiege, S. C., Heskel, M., Fan, Y. & Way, D. A. It's only natural: Plant respiration in unmanaged systems. *Plant Phys.* **192**, 710–727 (2023).

67. Groffman, P. M. & Fisk, M. C. Calcium constrains plant control over forest ecosystem nitrogen cycling. *Ecology* **92**, 2035–2042 (2011).

68. Shao, S. et al. Long-term responses in soil solution and stream-water chemistry at Hubbard Brook after experimental addition of wollastonite. *Environ. Chem.* **13**, 528–540 (2015).

69. Li, W. & Johnson, C. E. Relationships among pH, aluminum solubility and aluminum complexation with organic matter in acid forest soils of the Northeastern United States. *Geoderma* **271**, 234–242 (2016).

70. Sridevi, G. et al. Soil bacterial communities of a calcium-supplemented and a reference watershed at the Hubbard Brook Experimental Forest (HBEF), New Hampshire, USA. *FEMS Microbiol. Ecol.* **79**, 728–740 (2012).

71. Sridhar, B. et al. Watershed-scale liming reveals the short- and long-term effects of pH on the forest soil microbiome and carbon cycling. *Environ. Microbiol.* **24**, 6284–6199 (2022).

72. Juice, S. M. et al. Response of sugar maple to calcium addition to northern hardwood forest. *Ecology* **87**, 1267–1280 (2006).

73. Groffman, P. M., Hardy, J. P., Driscoll, C. T. & Fahey, T. J. Snow depth, soil freezing, and fluxes of carbon dioxide, nitrous oxide and methane in a northern hardwood forest. *Glob. Chang. Biol.* **12**, 1748–1760 (2006).

74. Bailey, A. S., Hornbeck, J. W., Campbell, J. L. & Eagar, C. Hydrometeorological database for Hubbard Brook experimental forest: 1955–2000. U.S. Department of Agriculture, Forest Service https://doi.org/10.2737/NE-GTR-305 (2003).

75. Burton, W. C., Walsh, G. J. & Armstrong, T. R. Bedrock geologic map of the Hubbard Brook experimental forest, Grafton County, New Hampshire. Open-File Report 2000-45-B. US Geological Survey https://doi.org/10.3133/ofr0045B (2000).

76. Nezat, C. A., Blum, J. D. & Driscoll, C. T. Patterns of Ca/Sr and 87Sr/86Sr variation before and after a whole watershed $CaSiO_3$ addition at the Hubbard Brook Experimental Forest, USA. *Geochim. Cosmochim. Acta* **74**, 3129–3142 (2010).

77. Peters, S. C., Blum, J. D., Driscoll, C. T. & Likens, G. E. Dissolution of wollastonite during the experimental manipulation of Hubbard Brook Watershed 1. *Biogeochemistry* **67**, 309–329 (2004).

78. Hughes, J. W. & Fahey, T. J. Litterfall dynamics and ecosystem recovery during forest development. *Forest Ecol. Manag.* **63**, 181–198 (1994).

79. Ni, X. & Groffman, P. M. Declines in methane uptake in forest soils. *Proc. Natl. Acad. Sci. USA* **115**, 8587–8590 (2018).

80. Durán, J. et al. Winter climate change affects growing-season soil microbial biomass and activity in northern hardwood forests. *Glob. Chang. Biol.* **20**, 3568–3577 (2014).

81. Jenkinson, D. S. & Powlson, D. S. The effects of biocidal treatments on metabolism in soil – V:A method for measuring soil biomass. *Soil Biol. Biochem.* **8**, 209–213 (1976).

82. Urbanksi, S. et al. Factors controlling CO_2 exchange on timescales from hourly to decadal at Harvard Forest. *J. Geophys. Res. Biogeosci.* **112**, G02020 (2007).

83. Palmer, S. M., Driscoll, C. T. & Johnson, C. E. Long-term trends in soil solution and stream water chemistry at the Hubbard Brook Experimental Forest: relationship with landscape position. *Biogeochemistry* **68**, 51–70 (2004).

84. R Core Team. R: A language and environment for statistical computing. R Foundation for Statistical Computing, Vienna, Austria. https://www.R-project.org/ (2020).

85. RStudio Team. RStudio: Integrated Development for R. RStudio, Inc., Boston, MA URL http://www.rstudio.com/ (2016).

86. Zeileis, A., Kleiber, C., Kraemer, W. & Hornik, K. Testing and dating of structural changes in practice. *Comput. Stat. Data Anal.* **44**, 109–123 (2003).

87. Zeileis, A., Leisch, F., Hornik, K. & Kleiber, C. strucchange: an R package for testing for structural change in linear regression models. *J. Stat. Softw.* **7**, 1–38 (2002).

88. Pinheiro, J., Bates, D., DebRoy, S., Sarkar, D. & R Core Team. nlme: Linear and Nonlinear Mixed Effects Models. R package version 3.1-148. https://CRAN.R-project.org/package=nlme (2020).

Acknowledgements

Author contributions

A.R.P. conducted data access and analysis, led synthesis and development of manuscript concepts, and wrote and revised the manuscript. All co-authors contributed to data synthesis, development of manuscript concepts, manuscript writing, and manuscript revision. C.T.D. designed and managed long-term lysimeter data collection; M.B.G. led lysimeter data interpretation; T.J.F. led long-term C cycle synthesis at the study site and C budget work; C.E.J. led forest floor carbon stock analysis; M.M.K.K. conducted forest floor sample collection and analysis; L.D.M. led soil core collection and microbial C cycle analyses; J.L.M. collected and interpreted in situ greenhouse gas flux data; P.H.T. led conceptual development of coupled C and N cycling elements of the work; A.M.U. Conducted data analysis of greenhouse gas flux trends; G.F.W. led field work for soil core collection and in-situ greenhouse gas measurements; P.M.G. designed and managed long-term soil core collection and in-situ greenhouse gas measurements.

Competing interests

The authors declare no competing interests.

Additional information